Journal of Power Sources 244 (2013) 552–556

Contents lists available at SciVerse ScienceDirect

Journal of Power Sources

journal homepage: www.elsevier.com/locate/jpowsour

Short communication

Lithium storage in reduced graphene oxides

Shin-Liang Kuo [a], Wei-Ren Liu [b,*], Chia-Pang Kuo [c], Nae-Lih Wu [c], Hung-Chun Wu [a]

[a] Material and Chemical Research Laboratories, Industrial Technology Research Institute, Hsinchu, Taiwan
[b] Department of Chemical Engineering, R&D Center for Membrane Center, Chung Yuan Christian University, Chung Li, Taiwan
[c] Department of Chemical Engineering, National Taiwan University, Taipei, Taiwan

HIGHLIGHTS

- The capacity and charge/discharge curves of reduced graphene oxide varied with reduction processes.
- The enhanced reversible capacity of RGO is mainly attributed to specific functionalities rather than large surface areas.
- Not all functionalities contribute to reversible capacity.

GRAPHICAL ABSTRACT

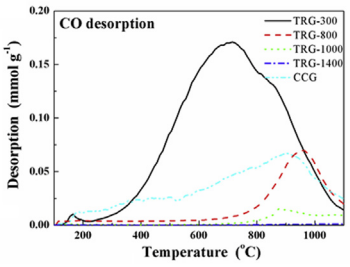

Sample	Surface Area ($m^2 g^{-1}$)	1st Charge (mAh g^{-1})	1st Discharge (mAh g^{-1})	Columbic Efficiency (%)
TRG-300	32.6	2080	1255	60.3
TRG-800	35.9	977	542	55.5
TRG-1000	25.9	514	286	55.6
TRG-1400	9.5	302	230	76.2
CCG	314.9	1120	477	42.6

ARTICLE INFO

Article history:
Received 1 November 2012
Received in revised form
29 January 2013
Accepted 31 January 2013
Available online 9 February 2013

Keywords:
Reduced graphene oxide
Lithium storage
Lithium battery
Anode

ABSTRACT

Reduced graphene oxides have been prepared via controllably thermal and chemical reduction processes. The structure, surface chemistry and electrochemical behaviors of reduced graphene oxides are investigated by Raman spectroscopy, N_2 adsorption, temperature-programmed desorption, Fourier-transform Infrared spectroscopy, X-ray photoelectron spectroscopy, as well as charge/discharge measurements. The enhanced reversible capacity of reduced graphene oxides is attributed to specific functionalities rather than to exceptional large specific surface area or structure defect. The contributed capacities at potential higher than 1.5 V and in region of 0.8–1.5 V are attributed dominantly to phenol groups and cyclic edge ether groups, respectively. These findings may be beneficial to the material design of graphene-based anode materials with high energy density.

1. Introduction

Graphene, one-atom thick, two dimensional layer of sp^2-bonded carbon, has drawn much attention because of its unique structure and fascinating electrical and mechanical properties. Graphene-based materials have also been suggested to be attractive candidates for potential applications in electrochemical energy storage. In particular, pure graphene, graphene-derivatives [1–7] and graphene composites [8–12], such as SnO_2/graphene and Si/graphene, have been suggested to serve as high-capacity anode materials for Li-ion batteries (LIB).

However, the electrochemical properties and origin of enhanced capacity for graphene-based LIB anode materials, including single- and multi-layered graphene and reduced graphene oxides (rGOs), have not been elucidated. Inconsistencies in reversible capacity and redox plateau of graphene-based materials were encountered. The capacity of graphene-based materials has been reported in the wide range of 200–1264 mAh g^{-1} within extended potential window of 3.5 V [1–4]. Most studies attribute the enhancement in capacity of graphene-based materials to the unusual large surface area and larger d-spacing, which is suggested to provide excessive active sites to accommodate higher Li uptake than LiC_6.

* Corresponding author. Tel.: +886 3 265 4140; fax: +886 3 265 4199.
E-mail addresses: WRLiu1203@gmail.com, wrliu@cycu.edu.tw (W.-R. Liu).

0378-7753/$ – see front matter © 2013 Elsevier B.V. All rights reserved.
http://dx.doi.org/10.1016/j.jpowsour.2013.01.186

However, even though super-dense LiC_2 prepared by ball milling and hydrogen containing carbon anodes have been shown to exhibit higher capacity, lithiation/de-lithiation process almost occurred below 1.0 V [13,14]. Therefore, there is no reasonable correlation between the electrochemical properties and properties of graphene-based materials.

Pan et al. [3] first discussed the effect of reduction process on electrochemical behavior of rGO nanosheets. They pointed out that the enhanced capacity was not fully determined by the d-spacing of graphene-based materials, nor affected by structure integrity. The surface structure defects could result in SEI formation and extra Li ion trapping, while the inner and edge structure defects could lead to reversible capacity. Pollark et al. [5] used chemical-vapor-deposition (CVD) graphene and *in-situ* Raman spectroscopy to investigate the lithiation/de-lithiation processes. The results showed that electrochemical properties of few-layer graphene were similar to those of graphite. Almost no intercalation process within high potential window (0.5–1.5 V) was observed, but the single-layer graphene was reactive with Li ion in wide potential range. In addition, first-principle calculation also suggests limited theoretical capacity due to strong Columbic repulsion force.

We have previously demonstrated that the specific surface area of rGO is not the critical factor for determination of both the capacity and reaction plateau [15]. In this study, systematical reduction processes were adopted on graphene oxides (GO) via either chemical or thermal reduction treatments. The relationship between structure properties and functionalities of rGO and corresponding electrochemical properties was established.

2. Experimental

2.1. Sample preparation

GO derived from SFG44 synthetic graphite powders (TIMCAL®) was synthesized by a modified Hummers' method [11]. 8.0 g synthetic graphite powder and 4.0 g $NaNO_3$ were put into 560 ml concentrated H_2SO_4 solution with stirring for 2 h. Then 32 g $KMnO_4$ was slowly added into the flask with ice bath for 2 h. The mixture was diluted by 800 ml de-ionized water. After that, 5% H_2O_2 was added into the solution until the color of the mixture changed to brown to ensure that $KMnO_4$ was fully reduced. The as-prepared GO slurry was re-dispersed in de-ionized water. Then, the mixture was washed with 0.1 M HCl solution to remove SO_4^{2-} ions. Finally, the GO solution was washed with distilled water to remove the residual acid until the solution pH reached ~5.

Two types of reduction processes were adopted for GO to form rGO. Thermally reduced graphene oxides (TRGs) were prepared by calcination at different temperatures under 15% H_2/N_2 atmosphere for 2 h with a heating rate of 0.5 °C min^{-1}. On the other hands, chemically converted graphene, named as CCG, was obtained by reduction with hydrazine under reflux at 100 °C for 24 h and subsequent drying at 100 °C in oven.

2.2. Electrochemical measurements

A two-electrode cell, coin cell 2032, was adopted for electrochemical characterization, using Li foil as the counter electrode and 1 M $LiPF_6$ in a 1:2 mixture of ethylene carbonate (EC) and ethyl methyl carbonate (EMC; Mitsubishi) as electrolyte. The working electrode was made of graphene-based material, Super-P (40 nm, TIMCAL®), and styrene–butadiene rubber/carboxymethyl cellulose (SBR/CMC) binder with weight ratio of 89/1/10. A constant current-constant voltage (CC–CV) charging mode and a constant current charging mode was adopted for charge (lithiation) and discharge (de-lithiation) processes, respectively. The operation voltage window is 0.005–3.5 V. The CC process employed a current of 0.1 mA mg^{-1}, while the CV process was operated at 0.005 V with a cut-off current of 0.03 mA mg^{-1}. Specific capacities are calculated based on the active-layer mass excluding binder and conductive additives.

2.3. Materials characterization

Brunauer–Emmet–Teller (BET) specific surface area was determined by N_2 adsorption on Micromeritics ASAP 2020. The structure of rGOs was characterized with μ-Raman spectroscope (Jobin Yvon T6400) with laser excitation (λ = 514.5 nm). Surface chemistry of graphene-based materials was characterized by X-ray photoelectron spectroscopy (XPS; INA-X), Fourier transform infrared spectrometer (FT-IR; Perkin Elmer/Spectrum 100) and temperature programmed desorption-gas chromatography (TPD-GC) using He as carrier gas.

3. Results and discussion

Fig. 1(a) and (b) shows the charge/discharge profiles and corresponding differential discharge capacity curves of TRGs and CCG. In comparison with pristine graphite, these rGOs exhibited much different electrochemical behaviors in either capacity or redox potentials. All the charge/discharge properties of the first cycle along with the corresponding BET specific surface area of TRG and CCG electrodes are listed in Table 1. To alleviate the effect of chemisorption or trap of Li ion on surface of materials, the thermal

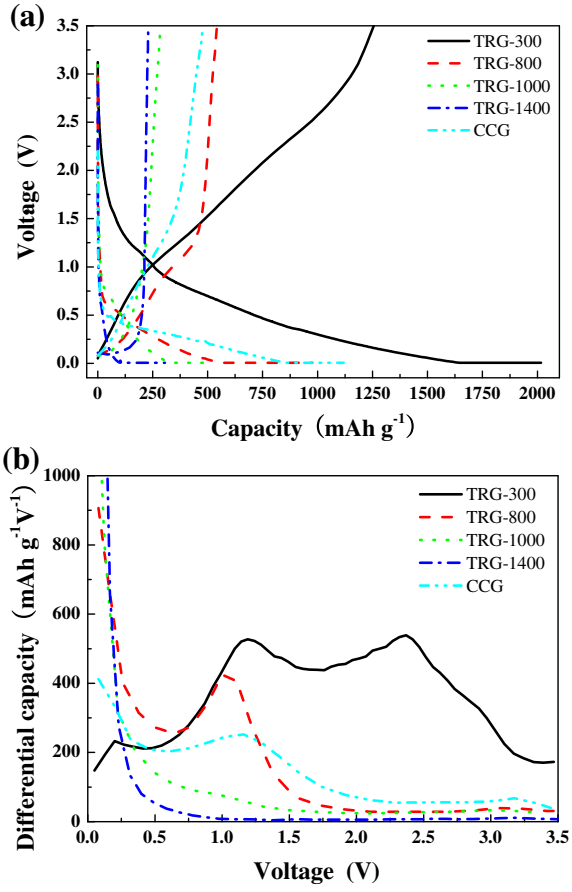

Fig. 1. (a) The charge/discharge curves of the first cycle and (b) the first corresponding differential de-lithiation curves of thermally and chemically reduced graphene oxides.

Table 1
BET surface area and the first charge/discharge cycle properties of different thermally and chemically reduced graphene oxides.

Sample	Surface area (m^2 g^{-1})	1st charge (mAh g^{-1})	1st discharge (mAh g^{-1})	Columbic efficiency (%)
TRG-300	32.6	2080	1255	60.3
TRG-800	35.9	977	542	55.5
TRG-1000	25.9	514	286	55.6
TRG-1400	9.5	302	230	76.2
CCG	314.9	1120	477	42.6

treatment with a small heating rate was adopted for TRGs to avoid thermal exfoliation. The BET surface area of present TRGs are less than 36 m^2 g^{-1}, which is much less than those prepared under rapid thermal exfoliation, typically greater than 300 m^2 g^{-1}. TRG-300 (the number denotes the final heat-treatment temperature) shows the largest capacity among these materials. The charge (lithiation) and discharge (de-lithiation) capacity of the first cycle for TRG-300 are 2080 and 1255 mAh g^{-1}, respectively, which led to the columbic efficiency of 60.3%. It is worth noticing that the reversible capacity exceeds the theoretical capacity of LiC_2, 1116 mAh g^{-1}, and lithiation/de-lithiation processes occurred across the entire potential range from 0.005 to 3.5 V. According to its differential capacity curve, the de-lithiation profile shows at least four peaks at ~3.0, 2.5, 1.2 and 0.2 V, respectively. Majority of the capacity occurs above 1.0 V. With increasing temperature of thermal treatment, a systematic change both in capacity and redox potential is observed. The reversible discharge capacity of TRG-800 decreases to 542 mAh g^{-1}, and the derivative profile shows only two major de-lithiation peaks respectively at 1.1 V and 0.15 V. The plateau at 0.15 V can be assigned to the typical intercalation between basal plans of graphite. The de-lithiation peak at 1.1 V was no longer observed for TRG-1000, while the capacity reduces to 286 mAh g^{-1}. As temperature of thermal treatment increases to 1400 °C, there is an obviously sharpening of the de-lithiation peak at 0.15 V, and only a capacity of 230 mAh g^{-1} is left. The CCG electrode exhibits similar electrochemical behaviors in both capacity and de-lithiation potential plateau, as indicated by derivative capacity curves, to those of TRG-800, even though CCG has a much greater, by more than eight folds, specific surface area (Table 1).

It has been proposed that GO has abundant oxygen-containing functional groups during chemical oxidation processes. However, the types and amounts of the functional groups left on the graphene-based materials vary with different oxidation/reduction conditions. TPD analysis is a typical method for quantitative and qualitative determination of functionalities of materials. All the oxygen-containing functional groups were thermally decomposed to release CO and/or CO_2 at different temperatures, and some are accompanied by H_2O due to interaction between adjacent functional groups. Fig. 2 shows TPD curves of TRGs and CCG, and the specific desorption amounts of CO and CO_2 are listed in Table 2. The thermal stability of oxygen-containing functional groups depends on types of functionalities and surroundings to which they are bounded. Even though major portion of the out-of-plane functional groups, including hydroxyl (C—OH), carboxyl (COOH) and epoxide (C—O—C), are removed under ~300 °C [16], broad desorption peaks of CO and CO_2 are still observed within range of 200–1100 °C in the TPD curve of TRG-300. The major CO desorption at region of 450–800 °C is typically attributed to phenol, ether, carbonyl, and quinone [16–18]. CO desorption at temperature less than 450 °C stems from the existence of phenol, aldehyde and carboxylic anhydride moieties. In addition, It is suggested that cyclic edge ether (pyrone) contribute to CO desorption high temperature region (>800 °C) due to its superior thermal stability. In addition,

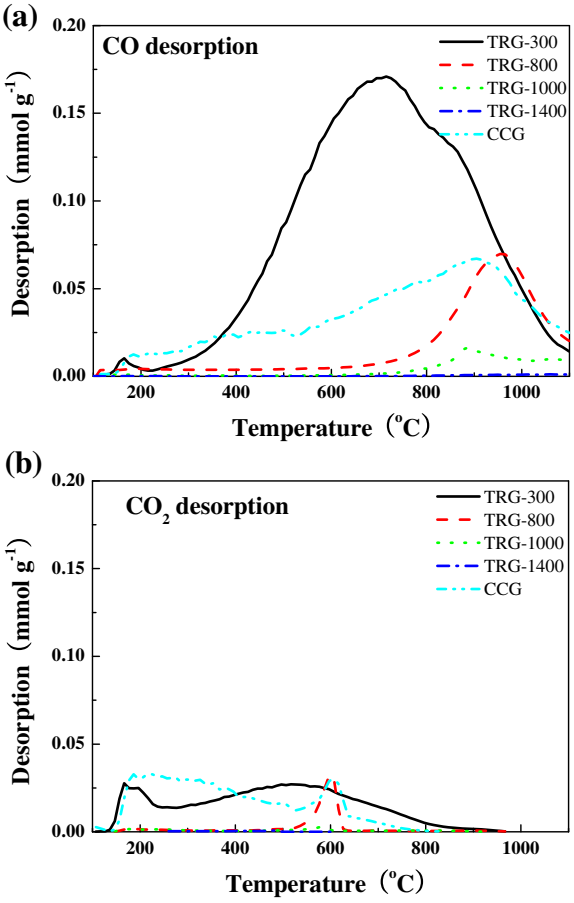

Fig. 2. Desorption of (a) CO and (b) CO_2 gases obtained during TPD analyses of thermally and chemically reduced graphene oxides at the corresponding temperature.

a relatively small amount of CO_2 desorption results from the decomposition of carboxyl and carboxyl anhydride groups at lower temperature region (<450 °C), as well as lactone groups for the higher temperature region. For TRG-800, majority of functional groups with lower thermal stability were removed and only desorption of cyclic ether and lactone was left. Almost no CO and CO_2 desorption for TRG-1000 and TRG-1400 was observed. On the other hand, due to the selective reduction of hydrazine, great reduction of CO desorption in the region of 400–900 °C and less change in CO_2 desorption were observed.

FT-IR spectra of as-prepared GO and rGOs are shown in Fig. 3. GO exhibited several characteristic absorption bands. The prominent broad band at 2900–3500 cm^{-1} is assigned to hydroxyl (C—OH) with all vibrations from H_2O and COOH. Absorption band peaked at ~1715 cm^{-1} and 1583 cm^{-1} corresponds to C=O stretching from carboxyl and lactone, and in-plane vibration of sp^2-hybrid C=C, respectively. In addition, the overlapped band at

Table 2
CO and CO_2 desorption amounts of different reduced graphene oxides.

Sample	CO desorption (mmol g^{-1})	CO_2 desorption (mmol g^{-1})	Total desorption (mmol g^{-1})
TRG-300	7.79	1.28	9.07
TRG-800	1.95	0.20	2.15
TRG-1000	0.52	0.06	0.58
TRG-1400	<0.10	<0.05	<0.15
CCG	3.65	1.20	4.85

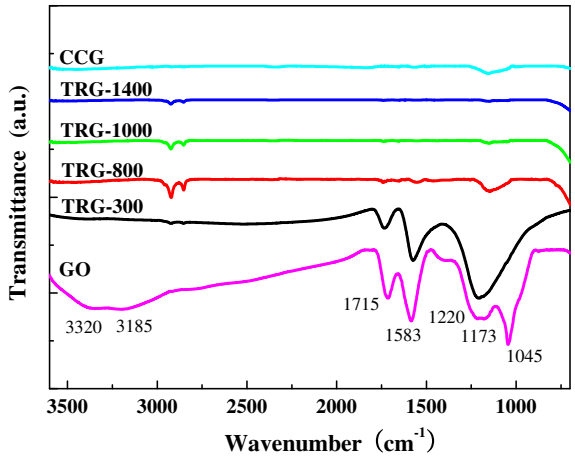

Fig. 3. FT-IR spectra of as-prepared GO and thermally and chemically reduced graphene oxides.

1100–1280 cm^{-1} is attributed of peroxide, ether, lactol, anhydride and epoxide groups [16]. A strong absorption peak at 1045 cm^{-1} could be related to stretching of C–OH and possible stretching of C–O in ether. As GO was reduced via thermal or chemical process, reduction of intensity of characteristic absorption peaks was observed. TRG-300 showed dramatic reduction in absorption bands at 3000–3500 cm^{-1}, ~1715 cm^{-1}, and 1045 cm^{-1}, indicating the loss of C–OH, COOH and H_2O. For both TRG-800 and CCG, most of absorption bands were diminished, and only a weak stretching peak at region of 1230–1025 cm^{-1} was left. In addition, almost no characteristic peaks were presented for TRG-1000 and TRG-1400.

Fig. 4(a) and (b) shows XPS spectra of C 1s and O 1s of TRGs and CCG respectively. The C 1s spectra were normalized by the C=C characteristic peak with binding energy of 284.5 eV. The C1s spectrum of TRG-300 shows three peaks assigned to oxygen functional groups, including C–O signals from phenol and ether at 286.1 eV, C=O from carbonyl and quinone at 287.5 eV, and –COO from carboxyl and ester at 288.7 eV. The relative intensity of C–O peak is much larger than those of C=O and –COOH. In addition, O1s spectrum of TRG-300 presents two characteristic peaks at 531.0 and 533.5 eV corresponding to O=C and O–C configurations, respectively. The intensity ratio of O–C and O=C peaks is ~2. On the other hand, strong reduction in all oxidative signals for TRG-800 and TRG-1400 was detected. The residual oxygen of TRG-800 is typically in form of O–C structure, which is consistence with that the main functionality is cyclic ether via TPD analysis. XPS spectra of CCG indicate that only the oxygen atoms in O–C environment is partially reduced, but no change in O=C configuration. It is suggested that hydrazine exhibits selective reduction capability on epoxide and phenol located at the interior of aromatic domain [19]. In comparison with TPD and XPS data of TRG-300 and CCG, major CO desorption at temperature region of 450–800 °C for TRG-300 is attributed to phenol group.

Structure integrity of graphitic materials was confirmed by Raman spectroscopy. As shown in Fig. 5, TRGs, and CCG all exhibited a strong D band at ~1350 cm^{-1} and a G band at ~1600 cm^{-1}, corresponding to sp^3 and sp^2 of carbon atoms, respectively. The existence of D band means defects are located in graphitic structure or edge. TRG-300, TRG-800, TRG-1000, and CCG showed similar Raman characteristics. The D/G ratio was calculated ranging between 0.85 and 1.1 and no 2D peaks at ~2700 cm^{-1} was presented. The lateral dimension of sp^2 graphitic domain was estimated to be ~2 nm using the correlation modified by Matthews et al. [20,21]. It is worth to note that no systematic change in D/G

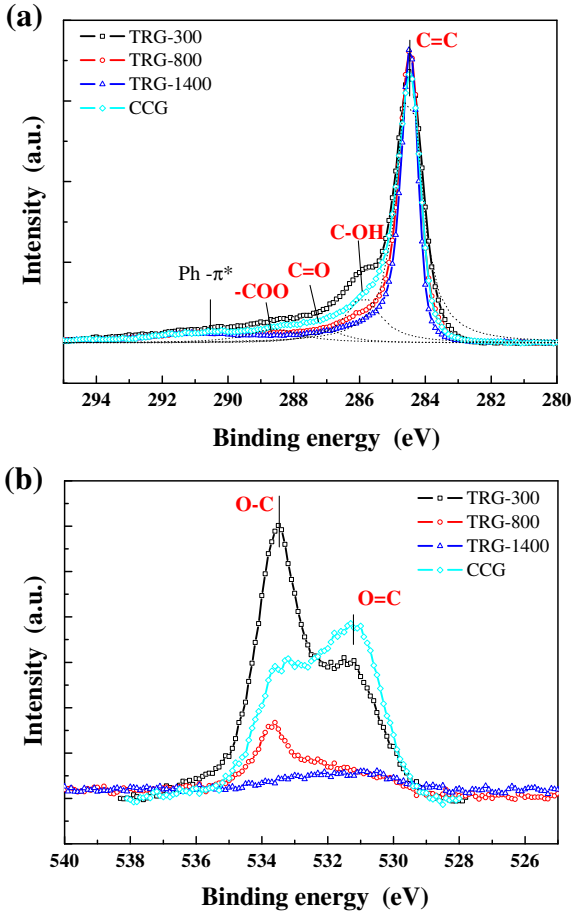

Fig. 4. XPS spectra of different thermally and chemically reduced graphene oxides: (a) C 1s spectra and (b) O 1s spectra.

ratio for TRG with heat treatment under 1000 °C was observed, indicating that a negligible expansion of sp^2 graphitic clusters in carbon matrix occurred even de-oxygenation was proceed under thermal and/or chemical reduction processes. The long-range graphitic crystallinity of rGOs derived from either low temperature thermal reduction or chemical reduction did not exist. On the other hand, TRG-1400 presented the D/G ratio of ~0.3, in accompany with decrease in FWHM of D and G peaks and appearance of

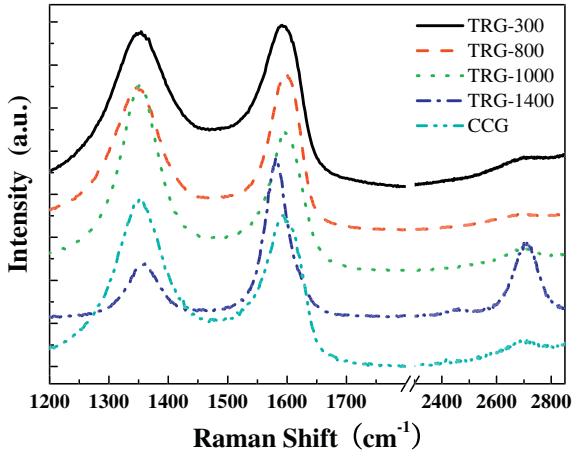

Fig. 5. Raman spectra of different thermally and chemically reduced graphene oxides.

2D peak. It is indicated that an obvious restoration of graphitic structure under higher temperature thermal treatment. The graphene domain size was calculated around 4 nm, which is 2 times of that for TRG-1000.

According to electrochemical properties and surface chemistry of different rGOs, some correlations were found. Redox reactions of TRGs and CCG not only occurred at carbon host structure, but also on the specified functional groups, even though the existence of functionalities could result in additional irreversible capacity. In comparison with the properties of TRG-1000, TRG-800 and CCG, the capacity derived from the redox couple centered at 1.1 V is attributed to the existence of cyclic edge ether which shows thermal stability higher than 800 °C. In addition, the capacity at potential region beyond 1.5 V could mainly correspond to lithiation/de-lithiation by phenol functionality according to properties of TRG-300, TRG-800 and CCG. However, the carboxylic, carbonyl and quinone moieties do not contribute to the capacity significantly according to the difference in functionalities distribution of TRG-800 and CCG. In addition, the discharge capacity occurred below 1.0 V resulted from the intercalation process of carboneous materials. For CCG and TRGs treated less than 1000 °C, the shoulder plateau at ~0.5–1.0 V is not correlated to functionality, but rather to sp^2–sp^3 carbon hybrid matrix. A significant change of charge/discharge curves from sloping potential curves to flat plateau at 0.15–0.2 V is attributed to the expansion of graphitic domain, which is consistent with value of typical graphitic anodes.

4. Conclusions

Differently reduced graphene oxides were prepared via controllably thermal and chemical reduction processes. The electrochemical properties and surface chemistry of TRGs and CCG were investigated. The results indicate that the enhanced reversible capacity of rGOs is mainly attributed to specific functionalities rather than large specific surface area or structure defects. The capacity at potential higher than 1.5 V is predominantly attributed to phenol groups, while the capacity derived from the redox couple at 1.1 V results from cyclic edge ether groups. In addition, some functional groups, such as carboxyl, lactone and carbonyl, do not result in reversible lithiation/de-lithiation processes.

Acknowledgments

The authors would like to thanks the financial support by Industrial Technology Research Institute (B301AR4P30 and C301AA5235). This research was also supported by National Science Council under contract no. of 101-2218-E-033-001, 101-3113-P-002-026 and 101-3113-E-002 -002.

References

[1] G. Wang, X. Shen, J. Yao, J. Park, Carbon 47 (2009) 2049.
[2] P. Guo, H. Song, X. Chen, Electrochem. Commun. 11 (2009) 1320.
[3] D. Pan, S. Wang, B. Zhao, M. Wu, H. Zhang, Y. Wang, Z. Jiao, Chem. Mater. 21 (2009) 3136.
[4] P. Lian, X. Zhu, S. Liang, Z. Li, W. Yang, H. Wang, Electrochim. Acta 55 (2010) 3909.
[5] E. Pollak, B. Geng, K.-J. Jeon, I.T. Lucas, T.J. Richardson, F. Wang, R. Kostecki, Nano Lett. 10 (2010) 3386.
[6] C. Uthaisar, V. Barone, Nano Lett. 10 (2009) 2838.
[7] L. Wan, Z. Ren, H. Wang, G. Wang, X. Tong, S. Gao, J. Bai, Diamond Relat. Mater. 20 (2011) 756.
[8] S.-M. Paek, E. Yoo, I. Honma, Nano Lett. 9 (2009) 72.
[9] J. Yao, X. Shen, B. Wang, H. Liu, G. Wang, Electrochem. Commun. 11 (2009) 1849.
[10] X. Zhao, C.M. Hayner, M.C. Kung, H.H. Kung, Adv. Energy Mater. 1 (2011) 1079.
[11] K. Evanoff, A. Magasinski, J. Yang, G. Yushin, Adv. Energy Mater. 1 (2011) 495.
[12] J.K. Lee, K.B. Smith, C.M. Hayner, H.H. Kung, Chem. Commun. 46 (2010) 2025.
[13] R. Tossici, R. Janot, F. Nobili, D. Gue`rard, R. Marassi, Electrochim. Acta 48 (2003) 1419.
[14] N.A. Kaskhedikar, J. Maier, Adv. Mater. 21 (2009) 2664.
[15] S.-L. Kuo, W.-R. Liu, H.-C. Wu, J. Chin. Chem. Soc. 59 (2012) 1220.
[16] M. Acik, G. Lee, C. Mattevi, M. Chhowalla, K. Cho, Y.J. Chabal, Nat. Mater. 9 (2010) 840.
[17] S. Kundu, Y. Wang, W. Xia, M. Muhler, J. Phys. Chem. C 112 (2008) 16869.
[18] W. Shen, Z. Li, Y. Liu, Recent Pat. Chem. Eng. 1 (2008) 27.
[19] X. Gao, J. Jang, S. Nagase, J. Phys. Chem. C 14 (2010) 832.
[20] M.J. Matthews, M.A. Pimenta, G. Dresselhaus, M.S. Dresselhaus, M. Endo, Phys. Rev. B 59 (1999) R6585.
[21] G.A. Zickler, B. Smarsly, N. Gierlinger, H. Peterlik, O. Paris, Carbon 44 (2006) 3229.